Available online at www.sciencedirect.com
SCIENCE DIRECT®
International Journal of Heat and Mass Transfer 47 (2004) 5247–5256
International Journal of HEAT and MASS TRANSFER
www.elsevier.com/locate/ijhmt

A methodology to control direct-fired furnaces

Soumik Banerjee [a], Dipankar Sanyal [b], Swarnendu Sen [b], Ishwar K. Puri [a,*]

[a] *Department of Engineering Science and Mechanics, Virginia Tech, University of Illinois at Chicago, 223 Norris Hall MC 0219, Blacksburg, VA 24061, USA*
[b] *Department of Mechanical Engineering, Jadavpur University, Calcutta 700032, India*

Received 23 January 2004; received in revised form 11 June 2004

Abstract

A suboptimal control strategy to control heat treatment processes in a direct-fired batch type furnace is formulated. It minimizes deviations from a prescribed temporal load temperature profile and the energy input in terms of the fuel consumption. The control method requires a model for the heat transfer and combustion, which is described. Application of the method shows that the fuel input and heat transfer to the load can be controlled to maintain a specified instantaneous temperature. This is accomplished through a feedback loop that is constructed by comparing the desired and measured temperatures. A parametric study is conducted to demonstrate the model.
© 2004 Elsevier Ltd. All rights reserved.

Keywords: Furnace control; Combustion control; Heat transfer control

1. Introduction

Metallurgical heat treatment includes a set of important industrial processes that, in general, beneficially transform metal grain structure through imposed temperature changes. Through the process, metals are normalized, annealed, hardened or tempered so that they acquire specific properties. Heat treatment must be carefully controlled to ensure that the load follows a desired temporal temperature profile as closely as possible.

The heat treatment process inside a furnace can be performed either continuously or in batches by using hot combustion gases. The load in continuous furnaces moves through differentially heated zones. In contrast, the temperature in batch furnaces is generally varied by manipulating the heat supply rate. Direct-fired furnaces are generally of the batch type and a representative schematic is presented in Fig. 1. The dynamic load–temperature profile in a batch furnace can be established by controlling the fuel flowrate, which varies the combustion heat release rate. In this context, there are two important requirements, i.e., the fuel consumption must be minimized [1] and the temporal temperature profile of the load inside the furnace must follow the desired metal time–temperature changes as closely as possible. The temperature profile in industrial applications usually deviates from the desired values due to the complexities associated with heat transfer.

This paper presents a control strategy to simultaneously reduce the fuel consumption and minimize the deviations of the instantaneous load temperature from prescribed values during a heat treatment process. Our method is based on the constrained minimization

* Corresponding author. Tel.: +1 540 2313243; fax: +1 540 2314574.
E-mail address: ikpuri@vt.edu (I.K. Puri).

0017-9310/$ - see front matter © 2004 Elsevier Ltd. All rights reserved.
doi:10.1016/j.ijheatmasstransfer.2004.06.023

Nomenclature

a	preexponential factor for Arrhenius equation ($kg^{1.3}/m^{1.3}\,s$)
C_s	specific heat of solid (J/kg K)
C_v	specific heat of the product gas (J/kg K)
h	convection coefficient ($W/m^2\,K$)
Δh_r	heat of reaction (kJ/kg)
J	performance index
k	thermal conductivity (W/m K)
L	length (m)
$\dot{m}$	mass flowrate (kg/s)
n	number of internal elements inside the load
nl	number of elements inside the load
N	exponent
Nu	Nusselt number
$\dot{Q}'''$	rate of heat generation (J/s)
Re	Reynolds number
t	time (s)
δt	time step (s)
T	temperature (K)
T_a	activation temperature (E_a/R_u, K)
T_i	temperature of the ith element (K)
T_{ls}	temperature of the load surface (K)
$\mathbf{U}$	terminal weightage matrix
δv	volume (m^3)
$\mathbf{V}$	transient weightage matrix
$\mathbf{W}$	weightage on fuel minimization
Y_f	fuel mass fraction
Y_{in}	fuel mass fraction at furnace inlet

Greek symbols

ε	emissivity
λ	Lagrange multiplier
μ	viscosity of the product gas ($N\,s/m^2$)
ρ	density of the product gas (kg/m^3)
σ	Stefan–Boltzmann's constant (5.67×10^{8} W/$m^2\,K^4$)

Subscripts

g	gas
m	measured
n	non-measured
s	solid
t	total
x,y,z	along x,y,z axes, respectively

Superscripts

t	timestep
T	matrix transposition operator

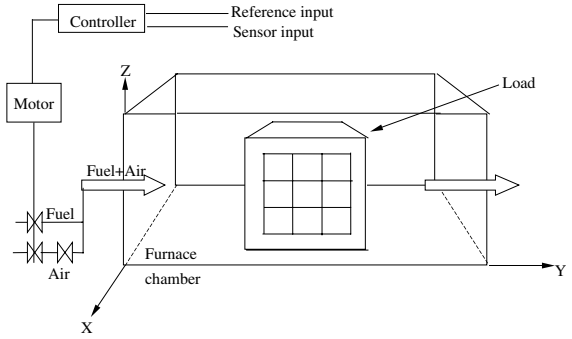

Fig. 1. Furnace geometry.

technique [2]. The desired system performance stipulates the control response speed, but care must be taken that fuel flow variations do not lead to combustion instabilities [3,4]. Whereas a fast response is required for applications such as gas turbines, which necessitates the use of robust control strategies [5], industrial furnaces have low frequency oscillations so that a slower response is permissible.

A process model for furnace heating is first developed. It considers combustion within the furnace ambient, heat transfer to the load and heat conduction within it. Our heat transfer analysis is based on a set of first order linearized dynamic equations according to a thermal network analysis [6]. We consider two-dimensional transient heat conduction within the load, assuming the third dimension to be sufficiently long. The process model provides the constraint equation to establish optimal control [7]. The fuel mass flowrate is obtained by minimizing the performance index with the constraints obtained from the process model. A sweeping method [8] is used for this purpose.

The control strategy described in this paper is general and applicable elsewhere, e.g., for general heating or quenching processes [9], accelerated cooling processes [10], minimizing the waste heat from an industrial process (for instance, in the steam or flue gas leaving a turbine), and optimizing the energy exchange at the blades of a turbine. Our work can be extended to develop a more powerful multiple input multiple output (MIMO) control method. Furthermore, the method is general; for instance, if electric current is considered as the output variable instead of temperature, it is applicable to many other problems of scientific and industrial value. One such example is power management for which grid scheduling is a dynamic problem. Here, the power loss must be optimized through the proper distribution of a single input current to several supply grids.

2. Mathematical model

2.1. Process model

We assume a load in the form of a square prism placed in a furnace with a uniform gas temperature. Strong stirring of the gases, e.g., through mechanical circulation, can maintain this temperature uniformity. Heating of the furnace walls and the low-density gases inside the furnace is neglected due to their small heat capacities relative to the load. Radiation heat transfer between the furnace and the load is considered, assuming thermal equilibrium between the furnace wall and the gases. A single-step global reaction is used to describe the combustion chemistry that occurs at a constant stoichiometry.

The furnace with the load inside, as shown in Fig. 1, is divided into several control volumes. We refer to these control volumes as elements. The furnace ambient consists of the gases and the wall as a single element. However, as shown in Fig. 1, the load is divided into several smaller elements to account for transient heat conduction. One of these elements is circumscribed by the load surface and the others are contained within it. The surface element is designated as the "first" element and there are $n \times n$ other elements within the load, as shown in Fig. 2. Each has a square cross-section and is identified by using integers 2 through $nl = n \times n + 1$. The load ambient, or the furnace wall and gas space combine, is the $(nl + 1)$th element. We assume that the furnace is insulated, making conduction losses at the walls negligible. The two sides of the load, with square section, are assumed to touch the insulated walls.

Convection and radiation heat transfer to the load are modeled through the state-space approach, i.e.,

$$\overline{\mathbf{M}}\dot{\mathbf{x}} = \overline{\mathbf{A}}\mathbf{x} + \overline{\mathbf{B}}\mathbf{u} \quad \text{for } t > t_1, \tag{1}$$

where $\mathbf{x}$ represents state variables (which are for the load the temperature field T_l, and for the load-ambient the temperature T_{nl+1} and the fuel mass fraction Y_{nl+1}), and $\mathbf{u}$ the control variable (which is essentially the mass flowrate $\dot{m}$ of the fuel–oxidizer mixture). The arrays $\mathbf{x}$ and $\mathbf{u}$ contain perturbation values that are deviations from their respective means. Representing the instantaneous values (with a caret) of the temperature, fuel mass fraction and fuel flowrate, respectively, in terms of their means (with an overbar) and perturbations,

$$T_t = \overline{T} + T, \quad Y_t = \overline{Y} + Y \quad \text{and} \quad \dot{m}_t = \dot{\overline{m}} + \dot{m}. \tag{2}$$

These variables can be expressed in the form

$$\mathbf{x}^T = [\,\mathbf{x}_1^T \quad \mathbf{x}_2^T\,], \tag{3a}$$

i.e.,

$$\mathbf{x}_1^T = [\{T_j\}_{j=1 \text{ to } nl}^T], \tag{3b}$$

$$\mathbf{x}_2^T = [\,T_{nl+1} \quad Y_{nl+1}\,] \tag{3c}$$

and

$$\mathbf{u} = u = \dot{m}. \tag{3d}$$

Here the superscript T is an operator that transposes matrices, and T_j represents the temperature of the jth element. Boldfaced notations are vectors or matrices and an italicized variable represents a scalar. In Eq. (1), $\overline{\mathbf{A}}$ and $\overline{\mathbf{B}}$ are coefficient matrices that contain mean terms and various geometrical parameters, such as the characteristic length and the dimensions of the load and the furnace. The mean values are held constant for the process and the deviations represent the perturbation values. The governing equations can be written in terms of these constant terms and the perturbation values, which are the variables used herein, using Eq. (2).

A single input single output (SISO) control strategy is developed, i.e., one input variable is manipulated to control a single output parameter. In our case, the single input is reactant mass flowrate and the output is the load

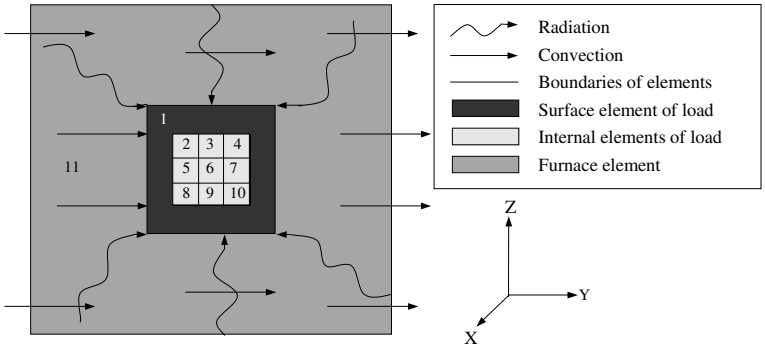

Fig. 2. Example problem.

surface temperature, monitored in practice with a thermocouple. The heat transfer is modeled in two dimensions by assuming negligible heat conduction along the z-axis. The load is centrally suspended inside the furnace. In accord with the network approach each element participates in heat transfer with all other control elements [6].

The spatial discretization of the continuum process model provides the matrices $\overline{\mathbf{M}}$, $\overline{\mathbf{A}}$ and $\overline{\mathbf{B}}$ in Eq. (1). The process model is represented by equations governing heat transfer for the load and the furnace elements. Their interface conditions are in terms of the load surface temperature T_{ls}. These governing equations are

$$\rho_{\mathrm{s}} C_{\mathrm{s}} \frac{\partial T_{\mathrm{s}}}{\partial t} = k_{\mathrm{s}} \left(\frac{\partial^2 T_{\mathrm{s}}}{\partial x^2} + \frac{\partial^2 T_{\mathrm{s}}}{\partial y^2} \right) \tag{4}$$

for the internal elements of the load,

$$k_{\mathrm{s}} \frac{\partial T_{ls}}{\partial \widehat{n}} = Q_{\mathrm{g}} = h(T_{nl+1} - T_{ls}) + 4\sigma\varepsilon(T_{nl+1}^3 T_{nl+1} - T_{ls}^3 T_{ls}) \tag{5}$$

for the surface element, and

$$\dot{\bar{m}} C_{\mathrm{p}} (T_{\mathrm{in}} - T_{nl+1}) + \dot{m} C_{\mathrm{p}} (\overline{T}_{\mathrm{in}} - \overline{T}_{nl+1}) + \Delta h_{\mathrm{r}} \Delta Y_{\mathrm{f}} = Q_{\mathrm{g}} 2L_x(L_y + L_z) \tag{6}$$

for the furnace element. The species equation, for the furnace element, has been formulated assuming the furnace to be a well-stirred reactor [11–14]. This relation is required to calculate the fuel consumption, and can be expressed as

$$\rho_{\mathrm{g}} (\delta v_{nl+1}) \frac{\mathrm{d}Y_{nl+1}}{\mathrm{d}t} = 0 = \dot{\bar{m}}(Y_{\mathrm{in}} - Y_{nl+1}) + \dot{m}(\overline{Y}_{\mathrm{in}} - \overline{Y}_{nl+1}) - \Delta Y_{\mathrm{f}}. \tag{7}$$

The symbol $\widehat{n}$ in Eq. (5) represents inward surface normal. In Eqs. (6) and (7), ΔY_{f} represents the linearized species destruction during combustion. For a stoichiometric or fuel–lean mixture, the total species destruction $\Delta Y_{\mathrm{f,t}}$ can be expressed as [15]

$$\Delta Y_{\mathrm{f,t}} = a(\delta v_{nl+1}) \rho_{\mathrm{g}}^N (Y_{nl+1})^N \exp(-T_{\mathrm{a}}/T_{nl+1}). \tag{8}$$

The linearized form of this relation is

$$\Delta Y_{\mathrm{f}} = a \cdot \delta v_{nl+1} \rho_{\mathrm{g}}^N (\overline{Y}_{nl+1})^{N-1} \times \exp(-T_{\mathrm{a}}/\overline{T}_{nl+1}) \left(N Y_{nl+1} + \overline{Y}_{nl+1} \frac{T_{\mathrm{a}}}{\overline{T}_{nl+1}^2} T_{nl+1} \right). \tag{9}$$

Spatial discretization of Eqs. (4)–(7) yields the following expressions for the perturbation variables

$$\begin{aligned} \rho_{\mathrm{s}} C_{\mathrm{s}} (\delta v_1) \frac{T_1^{t+1} - T_1^t}{\delta t} &= k_{\mathrm{s}} L_x \left(\sum_{j=1}^{n} T_{j+1} + \sum_{j=n^2-n+1}^{n^2} T_{j+1} - 2nT_1 \right) \\ &\quad + k_{\mathrm{s}} L_x \left\{ \sum_{j=2}^{n-1} T_{(j-1)n+2} + \sum_{j=3}^{n} T_{(j-1)n+1} - 2(n-2)T_1 \right\} \\ &\quad + 4Nuk_{\mathrm{s}} L_x (T_{nl+1} - T_1) + 4 \\ &\quad \times 2L_x(L_y + L_z)\sigma\varepsilon(\overline{T}_{nl+1}^3 T_{nl+1} - \overline{T}_1^3 T_1), \end{aligned} \tag{10}$$

$$\rho_{\mathrm{s}} C_{\mathrm{s}} \frac{T_j^{k+1} - T_j^k}{\delta t} = k_{\mathrm{s}} \left(\frac{T_{j+1} - 2T_j + T_{j-1}}{\Delta x^2} + \frac{T_{j+n} - 2T_j + T_{j-n}}{\Delta y^2} \right) \quad \text{for } j = 2 \text{ to } nl, \tag{11}$$

$$\begin{aligned} 0 &= \dot{\bar{m}} C_{\mathrm{p}} (T_{\mathrm{in}} - T_{nl+1}) + \Delta h_{\mathrm{r}} a \cdot \delta v_{nl+1} \rho_{\mathrm{g}}^N (\overline{Y}_{nl+1})^{N-1} \\ &\quad \times \exp(-T_{\mathrm{a}}/\overline{T}_{nl+1}) \left(N Y_{nl+1} + \overline{Y}_{nl+1} \frac{T_{\mathrm{a}}}{\overline{T}_{nl+1}^2} T_{nl+1} \right) \\ &\quad - 2L_x(L_y + L_z) h (T_{nl+1} - T_1) + \dot{m} C_{\mathrm{p}} (\overline{T}_{\mathrm{in}} - \overline{T}_{nl+1}) \\ &\quad - 4 \times 2L_x(L_y + L_z)\sigma\varepsilon(\overline{T}_{nl+1}^3 T_{nl+1} - \overline{T}_1^3 T_1) \end{aligned} \tag{12}$$

and

$$\begin{aligned} 0 &= \dot{\bar{m}}(Y_{\mathrm{in}} - Y_{nl+1}) + \dot{m}(\overline{Y}_{\mathrm{in}} - \overline{Y}_{nl+1}) \\ &\quad - a \cdot \delta v_{nl+1} \rho_{\mathrm{g}}^N (\overline{Y}_{nl+1})^{N-1} \times \exp(-T_{\mathrm{a}}/\overline{T}_{nl+1}) \\ &\quad \times \left(N Y_{nl+1} + \overline{Y}_{nl+1} \frac{T_{\mathrm{a}}}{\overline{T}_{nl+1}^2} T_{nl+1} \right). \end{aligned} \tag{13}$$

We have assumed a uniform temperature on the load surface by virtue of strong mixing of the gas flowing around the load. Since the conductivity of the load has been assumed to be directionally invariant, the instantaneous isotherms inside it do not remain parallel to the load surface. This does not allow rectangular shell-like elements to be used for internal discretization of the load. Instead, we use standard bar elements as shown in Fig. 2. In terms of 3×3 bar elements along x and y directions, this figure also depicts the indexing sequence used in the discretized Eq. (10). The heat transfer coefficients used in Eqs. (10)–(13) can be evaluated on the basis of an average Nusselt number [16].

We use the dimensionless forms of these matrices and vectors (Eqs. (14)–(16) below) in our analysis. The following transformations are employed to normalize the variables $\mathbf{x}$, $\dot{\mathbf{x}}$ and $\mathbf{u}$, namely,

$$\hat{\mathbf{x}} = \mathbf{x}/T_{\mathrm{fi}}, \tag{14}$$

$$\hat{\dot{\mathbf{x}}} = \dot{\mathbf{x}}/(T_{\mathrm{fi}}/\delta t) \tag{15}$$

and

$$\hat{u} = u/\dot{m}. \tag{16}$$

Here, T_{fi} represents the initial temperature of the furnace and δt the time interval for the process. The state space equation (Eq. (1)) is made dimensionless to facilitate a general control strategy. Therefore, the coefficient matrices on both sides of the state space equation are non-dimensionalized by dividing with the expression $\rho C_v(T_{fi}/\delta t)$. Henceforth, the bold capital letters **A**, **B** and **M** will represent the dimensionless forms for the matrices $\overline{\mathbf{A}}$, $\overline{\mathbf{B}}$ and $\overline{\mathbf{M}}$. Each row of the matrix in the state space equation (Eq. (1)) represents the energy equation for a separate element. It is developed by constructing the matrices $\overline{\mathbf{A}}$, $\overline{\mathbf{B}}$ and $\overline{\mathbf{M}}$ and the vectors **x**, $\dot{\mathbf{x}}$ and **u** based on Eqs. (10)–(13).

2.2. Control model

Metallurgical requirements limit the temporal variations in the reference (or ideal) load temperature $\mathbf{T}_R^t$ at different times. The deviation between the actual load temperatures and these reference values should be as small as possible, particularly during the soaking phase. If we divide the entire process into several time intervals, we can define two different temperature deviations for an interval. One is the deviation at the end of the interval ranging from initial time t_1 to final time t_2 and the other the corresponding sum over all discrete time steps within that interval. Both of these deviations must be minimized, as must the fuel consumption for the process. Therefore, we will define a performance index that contains all terms that are to be simultaneously minimized. To simplify the mathematical treatment the squares of these terms are used, which provide the simplest form that can be minimized. We represent the perturbation in the reference temperature by $\mathbf{T}_R$.

The three different variables to be minimized are

$$J_1 = \frac{1}{2}(\mathbf{D}\mathbf{x}(t_2) - \mathbf{T}_R(t_2))^T \mathbf{U}(t_2)(\mathbf{D}\mathbf{x}(t_2) - \mathbf{T}_R(t_2)), \tag{17a}$$

$$J_2 = \frac{1}{2(t_2 - t_1)} \int_{t_1}^{t_2} \{(\mathbf{D}\mathbf{x} - \mathbf{T}_R)^T \mathbf{V}(\mathbf{D}\mathbf{x} - \mathbf{T}_R)\}\, dt \tag{17b}$$

and

$$J_3 = \frac{1}{2(t_2 - t_1)} \int_{t_1}^{t_2} \{\mathbf{u}^T \mathbf{W}\mathbf{u}\}\, dt. \tag{17c}$$

The first relation (Eq. (17a)) represents the end state deviation. The matrix $\mathbf{T}_R$ contains the desired load element temperatures at any time during the process. The diagonal matrix **D** contains either a null value or "one" along its diagonal. It is used to determine the temperature deviation for the elements for which the temperature is measured by a sensor. Entries that equal "one" indicate the locations of the m states that are measurable in practical applications. For instance, it is possible that a sensor can measure only the load surface temperature and not the spatial temperature distribution within its bulk. Eq. (17b) represents the integrated deviation of the measured temperature from its desired value over the duration of the process. Again, matrix **D** denotes those elements for which temperature measurements are available. The third relation (Eq. (17c)) considers the total fuel consumption during the process. These three terms are combined in Eq. (17d) and minimized simultaneously using the state space equation as the constraint.

The performance index can thereafter be written in the form [17]

$$\begin{aligned} J &= J_1 + J_2 + J_3 \\ &= \frac{1}{2}(\mathbf{D}\mathbf{x}(t_2) - \mathbf{T}_R(t_2))^T \mathbf{U}(t_2)(\mathbf{D}\mathbf{x}(t_2) - \mathbf{T}_R(t_2)) \\ &\quad + \frac{1}{2(t_2 - t_1)} \int_{t_1}^{t_2} \{(\mathbf{D}\mathbf{x} - \mathbf{T}_R)^T \mathbf{V}(\mathbf{D}\mathbf{x} - \mathbf{T}_R) + \mathbf{u}^T \mathbf{W}\mathbf{u}\}\, dt. \end{aligned} \tag{17d}$$

We have employed the weighting matrices **U**, **V** and **W**, which have non-zero entries only at diagonal locations. The integrated expression (i.e., the second term on the RHS of the expression) is divided by a time difference to retain dimensional homogeneity for the terms contained in the performance index.

The relative importance of the terms in the cost function is allocated by varying the relative magnitudes of the diagonal elements of matrix **U** with respect to the corresponding values in the matrices **V** and **W**. The control performance can be evaluated by selecting different values of **V** and **W**, obtaining values of **U** for each chosen set and observing the response.

The performance index is minimized using the state space equation (Eq. (1)) as the constraint. Following the constrained minimization approach of introducing costates or Lagrangian multipliers λ [18], we obtain the following relations:

$$-\mathbf{M}^T \dot{\lambda} = \mathbf{A}^T \lambda + \mathbf{D}^T \mathbf{V}(\mathbf{D}\hat{\mathbf{x}} - \mathbf{T}_R) \quad \text{for } t \leqslant t_2, \tag{18a}$$

$$\hat{u} = -W^{-1} B^T \lambda \tag{18b}$$

and

$$\mathbf{M}^T \lambda(t_2) = \mathbf{D}^T \mathbf{U}(\mathbf{D}\hat{\mathbf{x}}(t_2) - \mathbf{T}_R(t_2)) = \mathbf{D}^T \mathbf{U}\mathbf{D}\hat{\mathbf{x}}. \tag{18c}$$

In Eqs. (18a) and (18b), the term $1/(t_2 - t_1)$ is incorporated within **V** and **W**. The regulatory control described in Eqs. (18a)–(18c) causes the perturbations at the terminal state of the process to approach zero. Details of this derivation can be obtained following the procedure described by Lewis and Syrmos [17]. Using the sweeping method [8], it is customary to extend Eq. (18c) over all times by removing the terminal time from the last expression to obtain

$$\mathbf{M}^{\mathrm{T}}\lambda = \mathbf{S}\hat{\mathbf{x}}, \quad \text{with } \mathbf{S}(t_2) = \mathbf{U}. \tag{19}$$

In obtaining the last equation in the form given, the matrix **D** has been chosen as a unitary matrix.

As noted earlier, due to the relatively small gas-phase density in comparison with the solid, the right-hand sides of Eqs. (12) and (13) are zero. Thus, in the state space equation (Eq. (1)), the row in matrix **M** corresponding to the energy equation for the furnace element has a null value, making that matrix singular. The control coefficient **B** also possesses a singularity, since the control variable of the reactant flowrate is a gas-phase variable and, hence, the rows corresponding to the load elements have null values. Thus, the energy equations corresponding to the nodes in the load and furnace are a set of dynamic equations that have time derivatives and which can be reduced to an algebraic relation. Consequently, Eq. (1) can be discretized and written in the form

$$\begin{bmatrix} \mathbf{M}_{\mathrm{l}} & 0 \\ 0 & 0 \end{bmatrix} \dot{\hat{\mathbf{x}}} = \begin{bmatrix} \mathbf{A}_{11} & \mathbf{A}_{12} \\ \mathbf{A}_{21} & \mathbf{A}_{22} \end{bmatrix} \begin{Bmatrix} \hat{\mathbf{x}}_1 \\ \hat{\mathbf{x}}_2 \end{Bmatrix} + \begin{Bmatrix} 0 \\ \mathbf{B}_2 \end{Bmatrix} \hat{u}. \tag{20}$$

We will exploit this structure by partitioning the matrices in Eqs. (18a)–(18c). Each matrix is expanded, yielding a pair of matrix equations through the partition. Subsequently, the equations are manipulated to eliminate variables and costates corresponding to the gas phase. Through this simplification, Eq. (20) assumes the form

$$\mathbf{M}_{\mathrm{l}}\dot{\hat{\mathbf{x}}}_1 = \widehat{\mathbf{A}}_{11}\hat{\mathbf{x}}_1 + \widehat{\mathbf{B}}\hat{u}, \tag{21}$$

where

$$\widehat{\mathbf{A}}_{11} = \mathbf{A}_{11} - \mathbf{A}_{12}\mathbf{A}_{22}^{-1}\mathbf{A}_{21} \quad \text{and} \quad \widehat{\mathbf{B}} = -\mathbf{B}_2\mathbf{A}_{22}^{-1}\mathbf{A}_{12}. \tag{22}$$

Comparing Eqs. (21) and (22) with their discretized counterparts, i.e., Eqs. (10)–(13), the following observations can be made. Matrix $\mathbf{M}_{\mathrm{l}}$ is diagonal and matrix $\mathbf{A}_{11}$ is diagonally dominant with its diagonal coefficients of equal magnitude but with opposite sign to the sum of all other elements in the same row. The matrix algebra corresponding to Eq. (22) leaves all coefficients other than in Row 1 unchanged. The Row 1 coefficients undergo modification due to substitution of Eqs. (12) and (13) in Eq. (10) to eliminate the gas-phase variables. In the process, the input control variable, i.e., the reactant mass flowrate, appears in the discretized representation of the temperature variation of the load surface element. The shell element responds to changes in the input variables. Since this element constitutes the boundary of the cluster of all other load elements, an element in the cluster is also bound to respond to a change in the input. This response occurs with a time delay that depends on the depth of the element in relation to the surface due to transient conduction. Clearly, Eq. (21) represents a system that is controllable. The matrix **A** is diagonally dominant and only a diffusive timescale is present for the problem. Thus, the system of equations is well posed and not stiff.

3. Results and discussion

3.1. Analytical results

Using the matrix splitting scheme of Eq. (20) along with the zero and non-zero splitting of **B** matrix, Eq. (18b) can be written as

$$\hat{u} = -\mathbf{W}^{-1}\mathbf{B}_2^{\mathrm{T}}\lambda_2 = \mathbf{W}^{-1}\left(M_{\mathrm{l}}^{-1}\widehat{\mathbf{B}}\right)^{\mathrm{T}}\mathbf{S}\hat{\mathbf{x}}_1. \tag{23}$$

To arrive at this relation, Eq. (18) and split forms of Eq. (19) (with the zero and non-zero parts of the mass matrix **M**) have been used. Further, using Eqs. (18a), (19), (21) and (23) and following the steps in Ref. [17], the Ricatti equation is obtained, namely,

$$-\dot{\mathbf{S}} = \left(\mathbf{M}_{\mathrm{l}}^{-1}\widehat{\mathbf{A}}_{11}\right)^{\mathrm{T}}\mathbf{S} + \mathbf{S}\mathbf{M}_{\mathrm{l}}^{-1}\widehat{\mathbf{A}}_{11} + \mathbf{S}\mathbf{M}_{\mathrm{l}}^{-1}\widehat{\mathbf{B}}\mathbf{W}^{-1}\left(\mathbf{M}_{\mathrm{l}}^{-1}\widehat{\mathbf{B}}\right)^{\mathrm{T}}\mathbf{S}, \quad t < t_2. \tag{24}$$

Eq. (24) is solved with the final condition provided by Eq. (19). Employing this solution in Eq. (23), the control parameter can be determined. This requires that all load states be measured. However, the temperature in practical furnaces can only be measured at some specific locations on the load surface, e.g., using thermocouples or imaging devices. As is evident from Eq. (23), the evaluation of the control strategy requires the online measurement of the vector $\hat{\mathbf{x}}_1$, which contains all of the load temperatures, both at the surface and in interior non-measured locations. For proper control, this online calculation of the states can be accomplished through reduced order modeling of Eq. (23) [19]. The reduced order method is an effective approach to deal with problems that provides real-time solutions of continuum systems.

Recently, Tiwari et al. [20] have demonstrated in the context of a glass cooling problem that sub-optimal control, which neglects the dependence of the control input on the subsurface temperatures, produces acceptable output variation that is in agreement with detailed numerical heat transfer modeling. Following a similar approach for obtaining suboptimal control, the matrices are decomposed further to distinguish between measured and non-measured locations, i.e.,

$$\mathbf{A}_{11} = \begin{bmatrix} \mathbf{A}_{\mathrm{mm}} & \mathbf{A}_{\mathrm{mn}} \\ \mathbf{A}_{\mathrm{nm}} & \mathbf{A}_{\mathrm{nn}} \end{bmatrix} \tag{25a}$$

and

$$\mathbf{M}_{\mathrm{l}} = \begin{bmatrix} \mathbf{M}_{\mathrm{m}} & \mathbf{0} \\ \mathbf{0} & \mathbf{M}_{\mathrm{n}} \end{bmatrix}. \tag{25b}$$

The subscripts m and n represent partitions corresponding to measured and non-measured load temperatures. Next, we obtain the sub-optimal control relation from Eq. (23) in the form

$$\hat{u} = K_0 \hat{\mathbf{x}}_{\mathrm{m}}, \tag{26a}$$

where

$$K_0 = \mathbf{W}^{-1}[\mathbf{M}_{\mathrm{m}}^{-1}\mathbf{B}_{\mathrm{m}}]^{\mathrm{T}}\mathbf{S}_{\mathrm{m}} \tag{26b}$$

denotes the gain constant. This constant can be utilized to determine the feedback gain as evident from Eq. (26a).

3.2. Example

A preliminary exercise to examine the applicability of the control strategy is conducted by evaluating the feedback gain constant K_0 and its response for a typical process by varying the magnitudes of the different weighting matrices and other physical parameters, such as the load and furnace dimensions. The major assumptions used in the model are as follows. The heat generation in the furnace element is assumed to occur due to the complete combustion of methane through a one step global reaction in a homogeneous mixture of fuel and preheated oxidizer. The gas-phase thermal conductivity, density and specific heat correspond to those for the burned gas temperature. The combustion heat generation is assumed to occur uniformly throughout the furnace volume and produce a uniform furnace temperature. Likewise, convective heat transfer is assumed to be uniform at all surfaces of the load. The average Nusselt number is defined as a function of the Reynolds and Prandtl numbers. Constant temperature furnace walls are assumed to radiate heat to the load, but the furnace gas is assumed to be a non-participating radiation medium. The wall temperatures are obtained by considering both radiation and convective heat transfer. The load surface element receives heat due to furnace wall radiation and convection from the combustion products. It conducts this heat into its interior. The heat transfer to the internal load elements from the surface element is modeled using two-dimensional transient heat conduction relations. Since the load has a large specific heat, the heat transferred through one side of an element is assumed to be quickly transferred to its other sides, thereby maintaining a uniform surface temperature. The weighting matrices determine the relative importance of the control objectives in the performance index [10]. A change in the furnace dimensions changes the Reynolds number and altering the width of the surface element modifies the heat capacity of this element.

The gain constant varies with time and can have negative values (as shown in Figs. 2–5) in contrast with classical PID-type control, which provides a time invariant

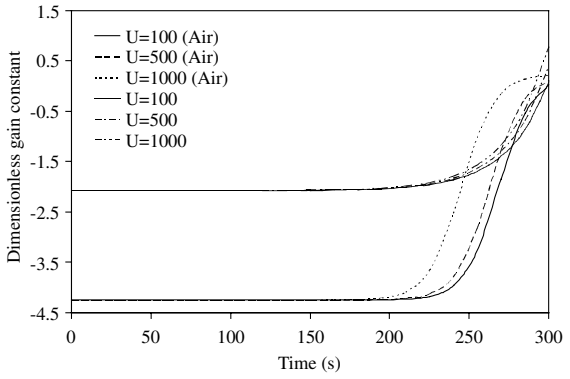

Fig. 3. Variation of gain constant with time for different **U**.

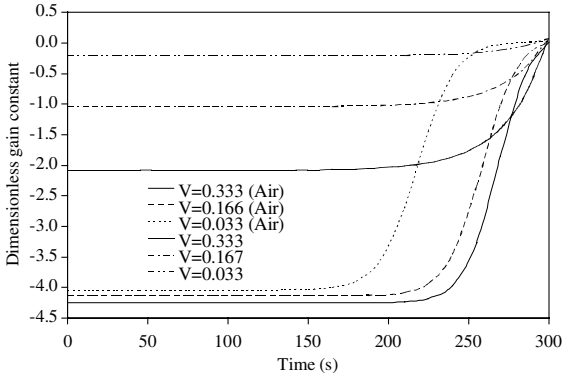

Fig. 4. Variation of gain constant with time for different **V**.

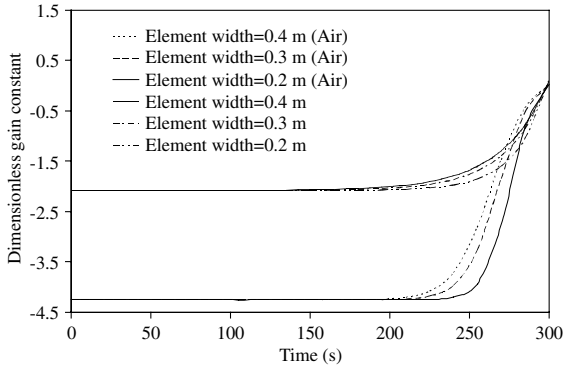

Fig. 5. Variation of the gain constant for different widths of the surface element.

feedback constant. This is clarified by examining Eq. (26a). If the actual load temperature at any instant is lower than the desired value, then the fuel flowrate must be increased in order to provide more combustion heat. Thus, the quantity $\hat{u}$ becomes positive or negative as the quantity $\mathbf{x}_{\mathrm{m}}$ has negative and positive values,

respectively. For this to occur, the gain constant K_0 should be negative.

As an example, we consider the heat treatment of steel that promotes steel hardness by changing its grain structure. It involves preheating, austenitizing, soaking and then cooling. Before austenitizing a steel load by heating it above 1000 K, it must be first preheated to remove these stresses. This involves initial heating in the range 500–700 K. For a representative analysis of the control method, we have considered accelerated preheating over this temperature range for 300 s. The oxidizer stream is assumed to consist of either air or pure oxygen that is preheated to 1473 K (1200 °C). In both cases, unheated methane (at 300 K) is assumed to mix with the oxidizer stream in near stoichiometric proportions and the mixture temperature is determined (1361 K for air and 1090 K for oxygen). The fuel mass fraction is 0.2 in case of oxygen as oxidizer and 0.055 when air is considered.

The heat treatment process inside a direct-fired furnace is simulated using MATLAB software. We have considered a steel load with a 1 m side (i.e., $L_x = L_y = L_z = 1$). The Reynolds number of the hot gas (that provides convective heat transfer to the load) is calculated on the basis of the load dimension, i.e.,

$$Re = \left(\frac{\dot{m}L}{A_f \mu}\right), \tag{27}$$

where A_f denotes the furnace cross-section area, L the load length and μ the viscosity of the flue gas. Thereafter, the Nusselt number is calculated. The furnace dimension characterizes the total amount of flue gas inside it and it is also used to determine the amount of heat released due to combustion. We will vary the furnace dimension to investigate its influence on the gain constant. The load and furnace gas properties and the combustion relations used in the simulation are provided in Table 1.

A mean fuel–oxidizer mixture flowrate is first calculated based on a lumped model analysis that assumes the total utilization of the combustion heat release. The product of the gain constant and the instantaneous temperature perturbation provides the required flowrate change from this mean value. The relation used for the lumped model analysis is

$$m_l C_s \frac{dT_l}{dt} = \dot{m} Y_f \Delta h_r. \tag{28}$$

The right hand side of this expression corresponds to the combustion heat release while the left side represents the amount of heat stored in the load. The fuel fraction in the gas mixture with a mass flowrate $\dot{m}$ is Y_f. The heat of reaction during combustion is Δh_r. There is an implicit assumption that the combustion heat release is entirely used to heat the load, which is considered as a lumped solid of mass m_l and specific heat C_s.

For a 200 °C temperature rise in 300 s when pure oxygen is used as oxidizer, the mean mixture mass flowrate is 0.23 kg/s (using Eq. (28)). Assuming system dependent losses of ~25%, a mass flowrate of 0.3 kg/s is used in the simulation. When a stoichiometric methane–air mixture is burned, the fuel mass fraction is 0.055. For this mixture, the total flowrate is 1.09 kg/s if the same fuel flowrate is used as for the pure oxygen example. The gain constant K_0 is calculated using Eq. (26b) and the variation of this constant during the process is presented in Figs. 3–6. Its value is used to determine the required fuel flowrate. We have used 11 elements for our simulation, 1 for the furnace element, 1 for the surface element of the load and 3×3 internal elements for the load. The computation time is fast, being ≈10 s with a Pentium IV 2.3 GHz processor.

Table 1
Load and flue gas properties

Load property	
Thermal conductivity	60.5 W/m K
Specific heat capacity	434.0 J/kg K
Density	7854.0 kg/m^3
Flue gas property	
Heat of reaction	50,016 kJ/kg
Preexponential factor	1.3×10^8 kg$^{1.3}$/m$^{1.3}$ s
Viscosity	5×10^{-5} N s/m^2
Activation temperature	24,358 K
Density exponent	−0.3

3.2.1. Gain constants

Comparisons have been made between the absolute values of the gain constants in order to have a physical insight into the change in the fuel flowrate. We first discuss the control method when pure oxygen is used as the oxidizer. An increase in the terminal weight produces a

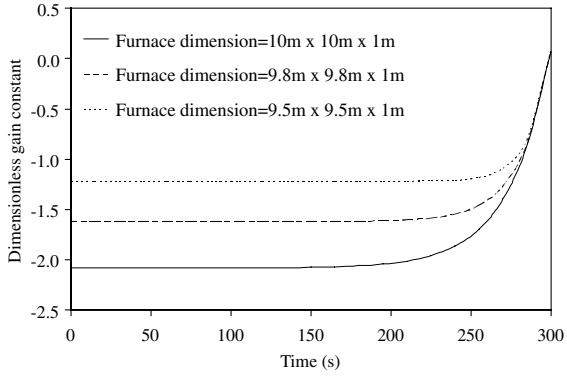

Fig. 6. Variation of gain constant with furnace dimensions.

smaller temperature deviation at the conclusion of the process. With the other two weighting matrices held constant, the value of the terminal weight matrix can be varied to determine its influence. To do so, **V** and **W** were assumed to have constant values of 0.33 and 0.033, respectively for a 0.3 m wide surface element. Fig. 3 shows that the dimensionless feedback gain constant has the same initial value for different values of **U** at the beginning of the process but decreases as the terminal state is approached. Eq. (26b) reveals that the gain constant K_0 varies with the value of $\mathbf{S}_m$, which is **U** (from Eq. (19)). Thus, a larger positive value for K_0 can be expected at the final state when a greater weightage is placed on **U**. Larger values of **U** produce a larger end state feedback gain constant at the end state. The gain constant's value decreases at earlier times for larger terminal deviation weights. The identical initial feedback constant values confirm that the **U** matrix only influences the process end state.

Likewise, the transient weighting matrix **V** can be changed with other matrices held constant. **U** and **W** were kept fixed with values of 100 and 0.033, respectively for a 0.3 m wide load. An increase in the weighting of **V** results in greater minimization of temperature deviations during the entire process. In this case, as the value of **V** is increased that of the gain decreases towards larger negative values as shown in Fig. 4. However, unlike the case for **U**, initial values of the gain constant are different for different weights. A larger gain constant implies a faster response to minimize temperature deviations at intermediate steps. This constant is larger when the weighting is increased, which also suggests that the fuel flowrate must be momentarily increased to minimize all intermediate temperature deviations during the process. Fig. 4 shows the relative importance of the weighting on the minimization of temperature deviations for the entire process.

The effect of a change in the surface element width (that is characteristic of all external load dimensions) on the dynamic feedback gain constant is presented in Fig. 5. Values of **U**, **V** and **W** are fixed at 100, 0.33 and 0.033, respectively. The gain constant value decreases with increasing dimension. The rate of this decrease is slightly different for the three element widths that are 0.1, 0.2 and 0.3 m. As the width increases, the load heat capacity increases, which improves response of the load to heating, which is reflected in the result. This can also be inferred from Eq. (26b), which shows that the gain constant is inversely proportional to the mass matrix $\mathbf{M}_{mm}$ corresponding to the measured nodes. As the surface width increases, the elements of the mass matrix have larger values, resulting in a smaller gain.

The effect of furnace dimensions is next investigated. The values of **U**, **V** and **W** are held at 100, 0.33 and 0.033, respectively for a 0.3 m load surface element width. As the furnace dimension increases, the gain constant becomes larger. For a fixed mass flowrate of the fuel–oxidizer mixture the convective heat transfer to the load decreases in larger furnaces as the Reynolds number decreases (cf. Eq. (27)). This is reflected through the smaller Nusselt number. For the same surface heat transfer to a specified load, a furnace with larger dimensions requires a higher combustion heat release rate, i.e., a larger fuel flowrate. This is clear in Fig. 6, which shows that the gain constant is larger for a larger furnace.

When air is employed as the oxidizer instead of pure oxygen, the nature of the various relations is essentially the same. The effect of various parameters on the gain constant for methane–air flames is discussed next. Fig. 3 shows the effect of the change of the terminal weightage matrix with time. In this case, the other weightage matrices **V** and **W** are held constant, as is the width of the surface element. As in the previous case with oxygen as the oxidizer, the gain constant decreases at earlier times and has a slightly larger end value when the terminal weightage is increased. That the initial values are identical irrespective of **U** confirms that the terminal state weightage matrix has an influence only during the terminal state.

Next, we examine the effect of changing **V** keeping **U**, **W**, the surface element width and the furnace dimensions constant. We again determine (in Fig. 4) that the initial gain constant increases with an increase in the weightage of **V** due to the larger corrections imposed for temperature deviations during all intermediate steps. Fig. 5 illustrates how the load surface element width influences the feedback gain constant when the weightage matrices and all other geometrical parameters are held constant. It, too, has the same nature and validates the applicability of this control strategy for various oxygen contents in the oxidizer stream.

Finally, a comparison is provided between the feedback gain constants in Fig. 7 when air and oxygen are

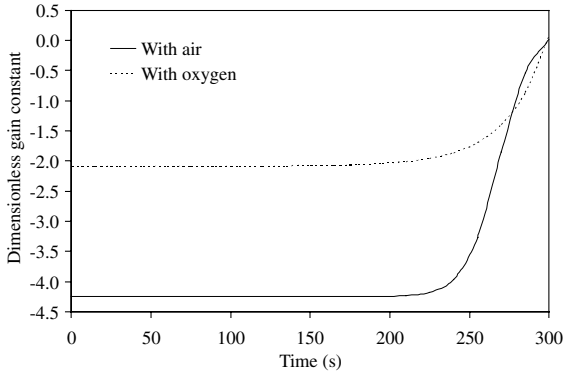

Fig. 7. Comparison of gain constant for different oxidizers.

used as the oxidizer. When all other parameters are held constant, the gain required in the case of air has a larger magnitude than for oxygen. This can be interpreted as follows. With oxygen as the oxidizer, the fuel mass fraction is 0.2 as compared to 0.055 for a methane/air mixture. A specified increase in the heat release rate requires that the fuel flowrate must be increased by a certain amount, which is a much larger proportion of the total mass flowrate in case of air than when oxygen is used as the oxidizer (cf. Eq. (26a)). Thus, for the same temperature deviation, the feedback gain to obtain an identical increase in the heat release rate is larger when air is used. This also offers qualitative validation of the control strategy.

4. Conclusions

We have shown that the response of a load to an external transient heat source can be represented through a feedback control structure. The formulated control strategy provides an offline determination of the values of the time-varying gain constant. This gain constant together with the real time temperature measurements of the load can be used to regulate a time varying fuel flow that is used to heat a load along a specified temporal temperature profile. In this manner, the load temperature can correspond to the desired temperature at any intermediate time or at the end of the process closely. The importance of a judicious selection of the weighting matrices involved in the control process is demonstrated.

We are able to minimize temperature deviations and the fuel flowrate simultaneously using a suboptimal strategy. The control strategy is validated through a parametric study that varies the weightage matrices, the load dimension and the furnace geometry. It reveals that while an increase in the transient weightage results in a larger initial gain value, an increase in the terminal weightage results in a higher gain constant at the terminal state. An increase in the thickness of the surface element produces a gain curve that diminishes rapidly in value while an increase in the furnace dimension results in a higher initial gain. Simulations performed to calculate the gain constant show that the control strategy can be applied irrespective of the content of the oxidizer stream.

Acknowledgment

This research is supported by the NSF/EPA Technology for a Sustainable Environment Program (through the NSF Thermal Transport and Thermal Processing Program) for which Dr. Richard Smith is the Program Director.

References

[1] J. Ford, A.J. Griffiths, J.A. Brandon, Estimating optimal open-loop controls for industrial batch heating plant, Proc. Inst. Mech. Eng. 214 (Part C) (2000) 1079–1097.
[2] S.K. Kim, D. Kim, I.M. Daniel, Optimal control of accelerator concentration for resin transfer molding process, Int. J. Heat Mass Transfer 46 (2003) 3747–3754.
[3] L. Crocco, Theoretical studies on liquid-propellant rocket instability, Proceedings of the Combustion Institute 10 (1965) 1101–1128.
[4] A.A. Putnam, in: J.M. Beer (Ed.), Combustion Driven Oscillations in Industry, American Elsevier, NY, 1971.
[5] B.S. Hong, V. Yang, A. Ray, Robust feedback control of combustion instability with modeling uncertainty, Combust. Flame 120 (2000) 91–106.
[6] M.V. Papalexandris, M.H. Millman, Active control and parameter updating techniques for nonlinear thermal network models, Comput. Mech. 27 (2001) 11–22.
[7] H.E. Pike, S.J. Citron, Optimization studies of a slab reheating furnace, Automatica 6 (1970) 41–50.
[8] A.E. Bryson, Y.C. Ho, Applied Optimal Control, Hemisphere, New York, 1975, pp. 151–153.
[9] B. Guerrier, C. Benard, Two-dimensional linear transient inverse heat conduction problem: boundary condition identification, J. Thermophys. Heat Transfer 7 (3) (1993) 472–478.
[10] S.K. Biswas, S.-J. Chen, A. Satyanarayana, Optimal temperature tracking for accelerated cooling processes in hot rolling of steel, Dyn. Control 7 (1997) 327–340.
[11] T. Hasegawa, S. Mochida, A.K. Gupta, Development of advanced industrial furnace using highly preheated combustion air, J. Propul. Power 18 (2) (2002) 233–239.
[12] R. Weber, S. Orsino, N. Lallemant, A. Verlaan, Combustion of natural gas with high-temperature air and large quantities of flue gas, Proceedings of the Combustion Institute 28 (Part 1) (2000) 1315–1321.
[13] R. Weber, A.L. Verlaan, S. Orsino, N. Lallemant, On emerging furnace design methodology that provides substantial energy savings and drastic reductions in CO_2, CO and NO_x emissions, J. Inst. Energy 72 (492) (1999) 77–83.
[14] A.M.A. Kenbar, S.A. Beltagui, T. Ralston, N.R.L. Maccallum, Measurement and modeling of NO(x) formation in a gas-fired furnace, Combust. Sci. Technol. 93 (1–6) (1993) 173–192.
[15] S. Park, A. Annaswamy, A. Ghoniem, Heat release dynamics modeling of kinetically controlled burning, Combust. Flame 128 (2002) 217–231.
[16] F.P. Incropera, D.P. DeWitt, Fundamentals of Heat and Mass Transfer, 2nd ed., John Wiley and Sons, 1990, p. 369.
[17] F.L. Lewis, V.L. Syrmos, Optimal Control, 2nd ed., John Wiley and Sons, 1995, pp. 152–153.
[18] K. Annamalai, I.K. Puri, Adv. Thermodyn. Eng., CRC Press, 2002, pp. 28–29.
[19] K. Ito, S.S. Ravindran, A reduced-order method for simulation and control of fluid flows, J. Comput. Phys. 143 (1998) 403–425.
[20] M.K. Tiwari, A. Mukhopadhyay, D. Sanyal, Numerical simulation of optimal multiple-input–multiple output control of impinging cooling of glass plate, Numer. Heat Transfer Part A 46 (4) (2004), in press.